Dalton Transactions

ROYAL SOCIETY OF CHEMISTRY

PAPER

View Article Online
View Journal

Cite this: DOI: 10.1039/d0dt01992e

Clever use of natural clay materials in the synthesis of non-symmetric carbonates by utilizing CO_2 as a feedstock: Ag/attapulgite nano-catalyst†

Ruixiang Guo,[a] Gang Wang[a,b] and Weisheng Liu *[a]

Received 4th June 2020,
Accepted 6th July 2020

DOI: 10.1039/d0dt01992e

rsc.li/dalton

Using natural minerals seems to be one of the most novel and environmentally friendly strategies to design catalysts for CO_2 conversion. Herein, we report a facile and efficient nano-catalyst for the synthesis of non-symmetric carbonate by utilizing a magnesium-aluminium silicate nano-mineral—attapulgite (ATP). Thanks to the unique structure of ATP and its ability to absorb carbon dioxide, the Ag/attapulgite nano-catalyst has excellent catalytic activity and stability in the carbon dioxide fixation reaction. The design of this Ag/attapulgite nano-catalyst provides a novel idea for realizing CO_2 conversion and clay resource utilization.

Introduction

It is mainly because of the use in some fine chemicals, drugs, and natural compounds that organic carbonate is an important intermediate in the petrochemical industry.[1] Moreover, compared with other organic carbonates, non-symmetric organic carbonates have more complex synthetic routes, more toxic synthetic processes, but more extensive uses.[2] Therefore, many people have studied the synthesis of non-symmetric carbonates. Dixneuf *et al.* first studied the related synthetic research,[3] which first synthesized cyclic carbonates under phosphine catalysis. Cyclocarbonates reacted with alcohols to form non-symmetric organic carbonates catalyzed by Et_3N or KCN. Costa *et al.* linked two reactions in series and reported that guanidine catalyzes the three-component synthesis of non-symmetric organic carbonates under supercritical CO_2 conditions.[4] In recent years, silver metal salts have been found to have excellent catalytic effects on the three-component reaction. Many systems have been developed, such as silver carbonate/triphenylphosphine,[1] silver chloride/ionic liquid,[5] silver sulfadiazine/tetrabutylammonium bromide.[6] These systems have high conversion under their own conditions, but they all have similar problems: low TOF value (turn over frequency) (Table S3†). To solve the problem, we take full advantage of attapulgite to design new catalysts for improving the utilization efficiency and catalytic efficiency of active substances.

Attapulgite (abbreviated hereafter as ATP) is a hydrous Mg- and Al-rich silicate clay mineral with a fibrous morphology.[8,9] Bradley *et al.* obtained the projection of ATP crystals (Fig. 1).[7] It can be seen that ATP forms a sandwich structure unit with two tetrahedral layers sandwiched with an octahedral layer.[8,10–16] This 2 : 1 structure determines that ATP has a large number of natural channels. The metal sites on the edge of the pores make the pores show weak alkalinity, which has a certain adsorption effect on acid gas.[17] In addition, recent studies have confirmed that ATP can effectively stabilize the inorganic nanoparticles loaded on it and control the size and particle size distribution.[18–21] Based on these characteristics of ATP, we designed a Ag/ATP composite nanocatalyst. Compared with the previous catalysts, the Ag/ATP catalyst has the advan-

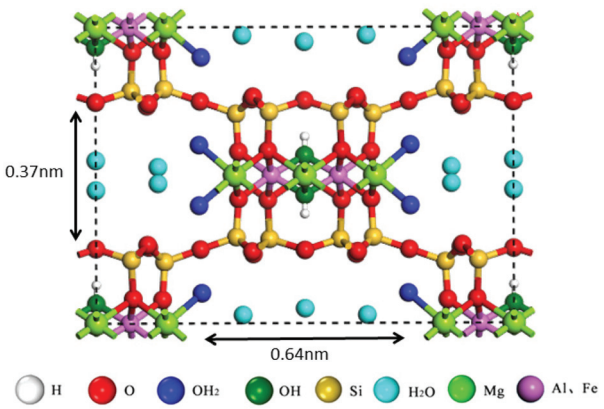

Fig. 1 Structure of attapulgite crystals.[7]

[a]Key Laboratory of Nonferrous Metal Chemistry and Resources Utilization of Gansu Province and State Key Laboratory of Applied Organic Chemistry, Key Laboratory of Special Function Materials and Structure Design, Ministry of Education, College of Chemistry and Chemical Engineering, Lanzhou University, Lanzhou, 730000, China. E-mail: liuws@lzu.edu.cn
[b]Lanzhou Petrochemical College of Vocational Technology, Lanzhou, 730060, China

†Electronic supplementary information (ESI) available. See DOI: 10.1039/D0DT01992E

tages of simple preparation, low amount of precious metals, mild catalytic conditions, and excellent catalytic performance. It is economical and provides a new way of environmental protection for CO_2 conversion and utilization.

Experimental section

Reagents and apparatus

Carbon dioxide (CO_2, 99%) was purchased from commercial sources and used without further purification. Attapulgite (ATP) was purchased from Jiangsu Jiuchuan Nanomaterials Technology Co. Ltd. The main chemical compositions are Al_2O_3 6.57%, MgO 27.20%, CaO 0.67%, SiO_2 49.64%, K_2O 1.47% and Fe_2O_3 5.64%. All the epoxides were bought from Sigma-Aldrich, Korea, and sodium hexametaphosphate (>99%) and zinc nitrate hexahydrate (>99%) were bought from Energy Chemicals Co. Ltd. 2-Methylimidazole was bought from TCI Chemicals. The infrared spectra were recorded using a Bruker VERTEX 70 FTIR spectrometer using KBr pellets in the 400–4000 cm^{-1} region. Nitrogen and carbon dioxide adsorption and desorption isotherms were measured at 293 K using a Micromeritics TriStar 3020 V1.04 system and the samples were degassed at 100 °C for 10 h before the measurements. The specific surface area was calculated using the Brunauer–Emmett–Teller (BET) method and the main pore size were analysed with the Barrett–Joyner–Halenda (BJH) method. The total pore volume was derived from the amount adsorbed at p/p^0 = 0.99. The elemental composition of the ATP was accurately analysed by an ICP-OES PQ9000 inductively coupled plasma optical emission spectrometer. The ^1H NMR data were collected using a JNM-ECS 400 M NMR spectrometer. Scanning electronic microscopy (SEM) images were obtained using an Apreo S electron microscope operating at 30 kV. Transmission electron microscopy (TEM) was performed using a Tecnai F30 and Talos F200S electron microscope operated in 300 kV. X-ray powder diffraction data were collected using a PANalytical X'Pert Pro diffractometer operated in 40 kV and 40 mA with Cu Kα radiation (λ = 1.5406 Å). Thermogravimetric analysis experiments were performed using a TGA/NETZSCH STA449C instrument heated from 25 to 800 °C (heating rate of 10 °C min^{-1}, a nitrogen atmosphere).

Preparation of Ag/ATP catalyst

Ag/ATP nanocomposites were prepared by a liquid phase method with silver contents of 1.0, 2.0, 3.0, 4.0, 5.0 and 6.0% (Table 1). The mixture of purified ATP (2.5 g), excessive sodium citrate, and silver nitrate was heated and refluxed in water (250 ml) for 4 hours. The product was centrifuged and washed with water (200 ml × 3). After freeze-drying, the black powder was collected for use.

Table 1 Preparation of Ag/ATP Catalyst

Sample	ATP/g	$AgNO_3$/g	$Na_3C_6H_5O_7{\cdot}2H_2O$/g
Ag/ATP-1	2.5	0.025	0.40
Ag/ATP-2	2.5	0.050	0.50
Ag/ATP-3	2.5	0.075	0.60
Ag/ATP-4	2.5	0.100	0.70
Ag/ATP-5	2.5	0.125	0.80
Ag/ATP-6	2.5	0.150	0.90

Verification of catalytic performance

Taking acetylene alcohol as an example, other experiments were similar. The mixture of acetylene alcohol (84.0 mg 1 mmol), 1,5-diazabicyclo-[4.3.0]-non-5-ene (abbreviated hereafter as DBN) (22.8 mg 0.15 mmol), Ag/ATP catalyst (5.0 mg) and DMF (1 mL) was added to the high-pressure steel kettle with PTFE liner. CO_2 gas (1 MPa) was filled into the kettle and reacted with a certain temperature for a specific time. After the reaction, the mixture in the reactor was taken out and the conversion rate was calculated by NMR (internal standard: TMS, test with deuterium reagent).

Results and discussion

Characterization of catalysts

It can be seen from Fig. 2 that ATP and Ag/ATP have similar infrared absorption characteristics, which indicates that there may be a physical interaction between Ag and ATP. At 3700–3200 cm^{-1} is the infrared absorption band of the stretching vibration of –OH, ≈3620 cm^{-1} is the stretching vibration of Al-OH or structural water, and 3545 cm^{-1} is the stretching vibration of (Al, Fe)O–H or (Fe, Mg)–OH.[22] The absorption band near 3400 cm^{-1} is that of physically adsorbed water (surface water and zeolite water).[22] The bending vibration of 1660 cm^{-1} is H_2O, and the strong spectral band appears at this position, which is caused by the overlap between the deformation vibration of coordination water and the deformation vibration of surface water or zeolite water.[19] There are 5–7 strong absorption bands between 1200–800 cm^{-1}, which are the symmetric and anti-symmetric stretching vibrations of Si–O, Si–O–Si and Si–O–Al.[19] The absorption band at

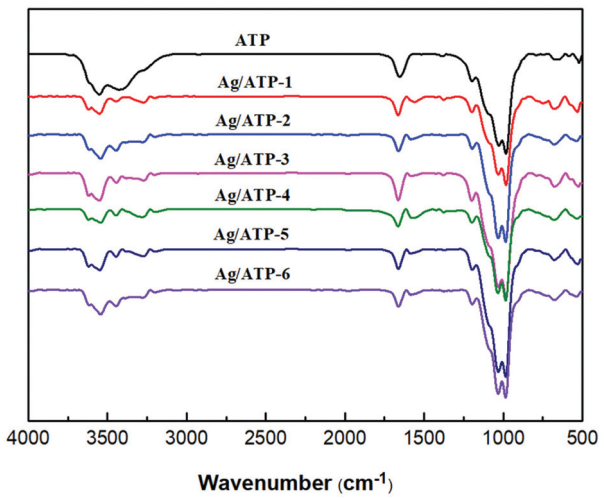

Fig. 2 IR spectra of ATP and Ag/ATP.

800–600 cm^{-1} is that of Si–O–Si symmetric stretching vibration and M–OH vibration. The absorption band at 600–400 cm^{-1} is mainly the coupling of Si–O distorted vibration, M–O vibration, and –OH plane vibration.[23–26] By comparing the spectra of ATP and Ag/ATP catalysts, the difference that the intensity of the Ag/ATP catalysts peaks changed in the range of 3200–3700 cm^{-1} was found. The reason for this phenomenon may be the loading of Ag nanoparticles, which results in the change of spectral peaks caused by the interaction of Ag^0 with structural water, crystalline water, or oxygen bridge.

The XRD patterns of ATP and Ag/ATP catalysts are shown in Fig. 3. Ag/ATP shows different diffraction peaks compared to ATP. ATP diffraction peaks appeared at 2θ = 8.42°, 13.64°, 16.32°, 19.8°, 27.56°, 35.0°. The 2θ = 8.31° diffraction peak is a characteristic peak of ATP, which is different from other minerals.[27] A diffraction peak at the position of 2θ = 38.14° (111), 64.55° (220), and 77.36° (311) (the position indicated by the diamond in the figure) indicates that silver has been successfully loaded onto the surface of the ATP.[28] The peak of silver in the spectrum is not obvious, which may be due to the low density of silver. Similar results have been reported before.[29] Besides, the result can be interpreted that ATP can disperse the silver better, making it difficult for XRD to detect the correlation peak of silver. Comparing the XRD spectra of the ATP before and after the Ag^0 loading, the ATP diffraction peak of Ag/ATP is consistent with ATP, indicating that the Ag/ATP prepared by this method does not change the original structure of ATP. At the same time, as the amount of Ag^0 loaded increases, the intensity of the characteristic diffraction peak of Ag^0 gradually increases.

According to the crystal structure of ATP, there are 4 types of water in ATP, including: surface adsorption water, pore adsorption water, crystal water, and structural water and its stability is gradually increased.[30] Similarly, the curves (Fig. 4 and Fig. S2†) show that when the temperature is less than

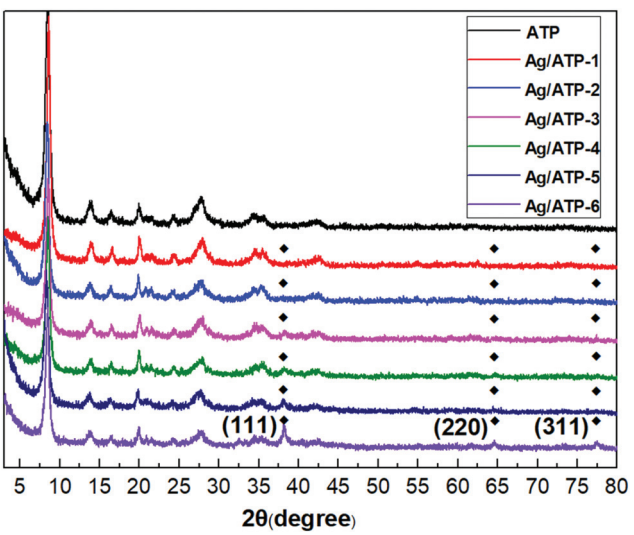

Fig. 3 XRD spectra of ATP and Ag/ATP.

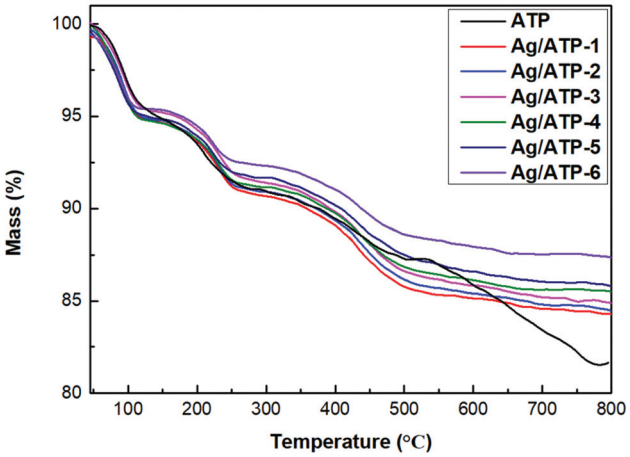

Fig. 4 The thermogravimetric analysis (TGA) curves of ATP and Ag/ATP catalysts.

120 °C, the change of weight loss curves is due to the removal of surface adsorption water and pore zeolite water; at 120 °C to 250 °C, the curve change is due to the removal of a part of the crystal water; the curve changes from 250 °C to 500 °C[30] is due to the removal of residual crystal water; from 500 °C to 700 °C, the curve change is due to the removal of structural water; then as the temperature increases, the curve of ATP and Ag/ATP catalyst tends to be stable, mainly because at high temperatures, the pore structure of ATP completely collapses to form silicate or sinter. The curve change of the series Ag/ATP catalyst tends to be stable after 600 °C.[31] The reason may be that due to the loading of the silver particles, the mass change caused by the removal of the structural water is small, and the curve change is not obvious. Moreover, with the increase in the loading of silver particles, the residual mass fraction of the material gradually increases after the curve is stabilized.

The BET isotherm adsorption analysis curves of ATP and Ag/ATP catalysts are shown in Fig. 5. It can be seen from the

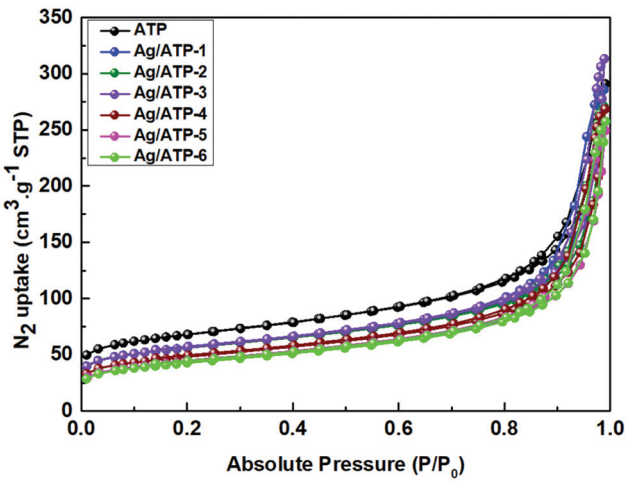

Fig. 5 BET isotherm curves of Ag/ATP.

Table 2 Pore structure parameters of ATP and Ag/ATP

Sample	S_{BET} ($m^2\ g^{-1}$)	V_{total} ($cm^3\ g^{-1}$)	V_{micro} ($cm^3\ g^{-1}$)	V_{ext} ($cm^3\ g^{-1}$)	PZ (nm)
ATP	223.9798	0.449962	0.042387	0.407575	13.6125
Ag/ATP-1	196.3714	0.442280	0.031595	0.410685	16.1668
Ag/ATP-2	195.4138	0.419625	0.031262	0.388363	15.5967
Ag/ATP-3	196.0432	0.484483	0.030039	0.454444	17.5063
Ag/ATP-4	169.8930	0.415718	0.023517	0.392201	16.3731
Ag/ATP-5	153.1387	0.385845	0.019890	0.365955	16.0530
Ag/ATP-6	150.0846	0.398666	0.018473	0.380193	16.9254

figure that when the relative pressure is low, the adsorption curve coincides with the desorption curve, indicating that a small amount of micropores existed; as the relative pressure increases, N_2 undergoes capillary condensation, and the isotherm rises rapidly due to capillary condensation. Hysteresis can be observed in this area, which is characterized by the presence of mesopores and micropores in the sample. The pore structure parameters of ATP and Ag/ATP catalysts are shown in Table 2. ATP has a large surface area (S_{BET}), which can provide adsorption centers and reactive centers for the catalytic reaction.[32] With the increase of silver loading, the S_{BET} and V_{total} of Ag/ATP tended to decrease, which may be caused by the formation of some pores blocked by silver nanoparticles.[33] It can be seen that after the loading of silver, the average pore diameter of the material increases slightly; the average pore diameter is between 15 and 18 nm, which is mesoporous. The reason may be that the surface structure of ATP is affected by the silver load.[15] The CO_2 isotherm adsorption of ATP and Ag/ATP catalyst was also measured (Fig. S1†). According to the IUPAC classification, the curve is a type 1 adsorption isotherm curve. For this adsorption model, the adsorption of CO_2 is closely related to pressure. With the increase of pressure, the adsorption capacity of CO_2 increases gradually. Combined with the results of the controlled experiment (Table 3, entries 4 and 5), it can be concluded that the CO_2 adsorption property of ATP plays an important role in the catalytic efficiency of the reaction.

The SEM photos in Fig. 6 clearly show the morphology of each material. We have observed that ATPs are mostly rod-shaped structures arranged irregularly, with a diameter of about 20–30 nm and a length of 0.1–1 μm (Fig. 6a–c). After silver was loaded on the ATP, no obvious silver nanoparticles were observed, and the overall structure of the ATP did not change significantly. Besides, with the increase in silver content, no large-scale agglomeration was observed in Ag/ATP-1, 2, 3, 4, and 5 (Fig. 6d–h). From the TEM photos, we can clearly see the pore structure of the ATP, whose diameter is less than 1 nm (Fig. 7a). This is consistent with the reported pore structure of ATP.[8] In another TEM image, we can clearly see that the silver nanoparticles are uniformly loaded on the ATP. The silver nanoparticles have a uniform size distribution and a diameter of about 2–3 nm. The surface structure of ATP was not changed after loading, and the pore structure of ATP was still observed (Fig. 7b). Many groups on the surface of the ATP are negatively charged, such as Si–OH, Al–OH, Si–O^- and Al–O^-. These groups can form stable nuclei during the formation of silver nanoparticles and protect the growth of silver nanoparticles.[22,34,35] Therefore, the ATP can effectively disperse and stabilize the silver nanoparticles.

Catalytic evaluation

We studied the catalytic ability of the Ag/ATP catalysts for non-symmetric organic carbonates and optimized the reaction conditions (Fig. S4–S10, Tables S1 and S2†). According to the good experimental results, the Ag/ATP-5 catalyst was used for the following experiments.

Control experiments show that Ag/ATP-5 requires DBN as a co-catalyst to perform asymmetric synthesis. Specifically, the reaction cannot be catalysed by Ag/ATP-5 and DBN alone (Table 3, entries 1–3). Moreover, the silver element without the load cannot be effectively catalyzed (Table 3, entries 4 and 5). We used Ag/ATP-5 as the catalyst (10 mg), DBN (0.3 mmol) as a cocatalyst, and catalyzed substrate 1 (2.8 mmol) with 2 (2 mmol) and CO_2 (1 MPa) to give a non-symmetric carbonate at 50 °C. After 6 hours of reaction, the yield reached 99% (Table 3, entries 5). After the ICP test (Fig. S3†), 2.68 wt% of the silver content was obtained, and the TOF value was 132 (h^{-1}). The catalytic efficiency of Ag/ATP is much higher than that of some metal salt catalytic systems (Table S3†). As a result, this shows that Ag/ATP-5 has good catalytic activity and meets the requirements of our design.

Table 3 Reaction of CO_2, 2-methyl-3-butyn-2-ol (**1a**) and benzyl alcohol (**2a**) in various catalyst systems by Ag/ATP-5[a]

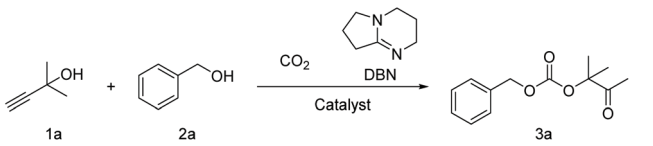

Entry	Catalyst	Co-catalyst	Solvent	T (°C)	Yield[d] (%)
1	Ag/ATP-5	—	DMF	60	—
2	—	DBN	DMF	60	2
3	Ag/ATP-5	DBN	DMF	60	99
4[b,c]	Ag	DBN	DMF	50	11
5[b]	Ag/ATP-5	DBN	DMF	50	99

[a] Reaction conditions: 3 mmol **1a**, 2 mmol **2a**, 10 mg catalyst, 0.3 mmol cocatalyst, 1 mL solvent, 6 h, 1 MPa CO_2. [b] 2.8 mmol **1a**. [c] 1 mg catalyst. [d] Conversions were determined with ^1H NMR analysis.

The reactions of CO_2 with a range of different substituted substrates were then conducted in the Ag/ATP&DBN catalyst system. At the outset, the effect of different propargylic alcohols on the reaction was studied. And the reaction had good adaptability to some primary alcohols and could achieve high yields (Table 4, entries 1–4). Further experiments showed that the reaction was sensitive to the steric hindrance effect of replacing R^1 and R^2. When R^1 and R^2 are large sterically hin-

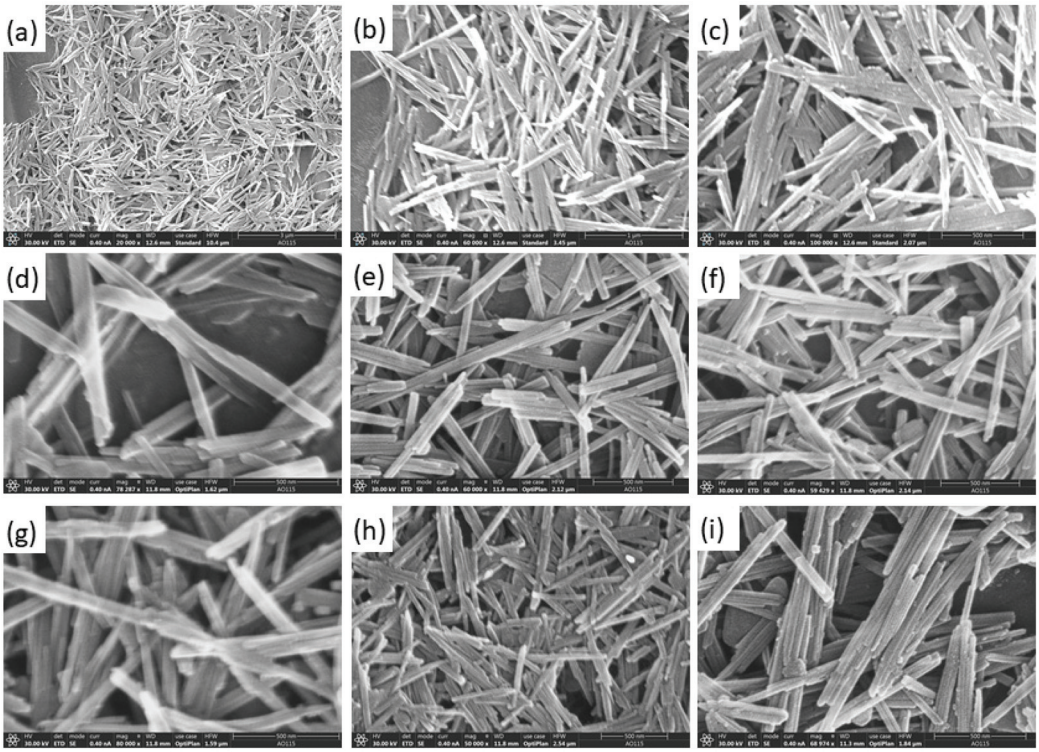

Fig. 6 SEM pictures of (a–c) ATP; (d) Ag/ATP-1; (e) Ag/ATP-2; (f) Ag/ATP-3; (g) Ag/ATP-4; (h) Ag/ATP-5; and (i) Ag/ATP-6.

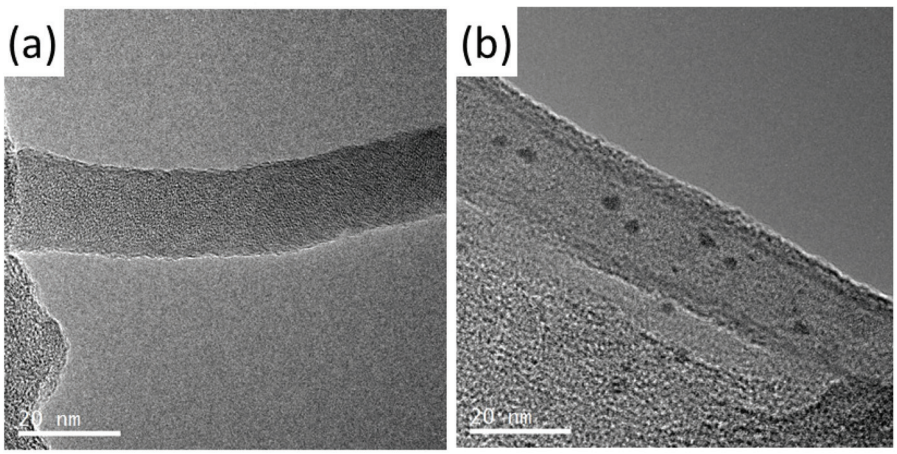

Fig. 7 TEM pictures of (a) ATP; (b) Ag/ATP-5.

dering groups, the yield of the reaction under the same conditions is greatly reduced (Table 4, entries 5). In addition, a substrate expansion study was conducted on primary alcohols. Next, the effect of primary alcohols was examined on the reaction. Evidently, the conversion rate of the reaction of the system depends on the electron donating ability of R^3. With the alkyl chain growth, its electron donating ability is enhanced, which causes the yield increase (Table 4, entries 6–8). The reason may be related to the stability of the alkoxy group formed after the DBN captures the hydrogen of the alcoholic hydroxyl group. As a result, we speculate that DBN, after capturing the hydrogen of the alcoholic hydroxyl group, activates the hydroxyl group as an important step in the reaction.

In order to verify the activation of hydroxyl groups by DBN, we used ^{1}H NMR (Fig. S11†). After the activation of DBN, the peaks of the alcoholic hydroxyl groups of **1a** and **2a** all move toward the high field, the peak shape changes, and the peak width increases. This is because the nitrogen heteroatom on

Table 4 Scope of the propargylic alcohols and primary alcohols substrates for the reaction[a,c]

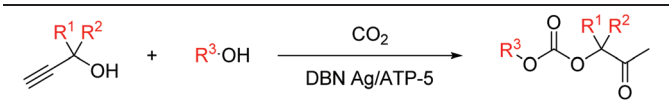

Entry	Propargylic alcohols	Primary alcohols	Product	Yield[b] (%)
1			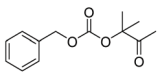	99
2			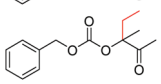	90
3			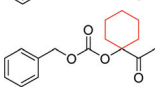	70
4	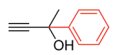		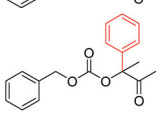	50
5	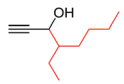		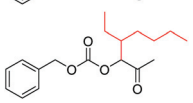	21
6			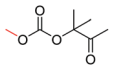	3
7			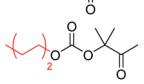	50
8			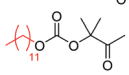	76

[a] Reaction conditions: 2.8 mmol propargylic alcohols, 2 mmol primary alcohols, 10 mg Ag/ATP-5, 0.3 mmol DBN, 1 mL DMF, 6 h,50 °C, 1 MPa CO_2. [b] Conversions were determined with ^{1}H NMR analysis. [c] All ingredients are racemic mixtures.

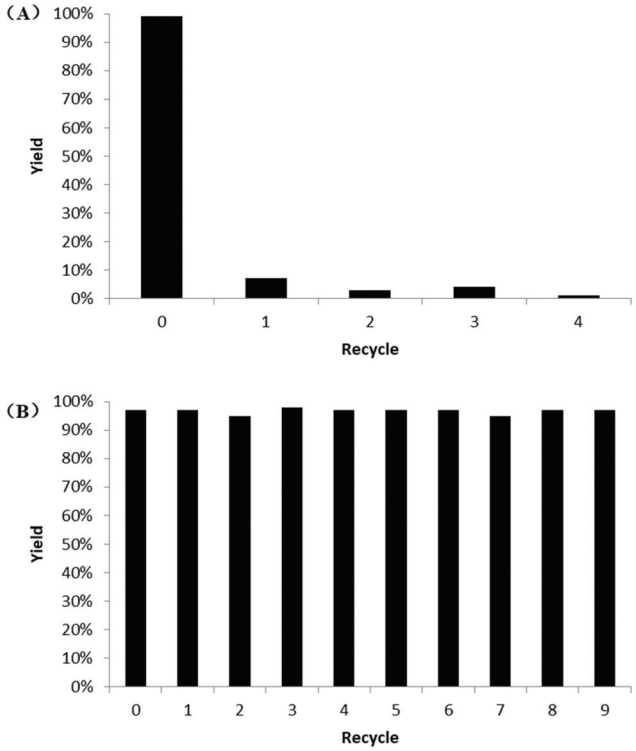

Fig. 8 Catalytic performance of Ag/ATP in subsequent reaction cycles; (A) 50 °C; and (B) 90 °C. Other reaction conditions: (A) 2.8 mmol **1a**, 2 mmol **2a**, 10 mg catalyst, 0.3 mmol cocatalyst, 1 mL solvent, 6 h, 1 MPa CO_2; (B) 8.0 mmol **1a**, 2 mmol **2a**, 10 mg catalyst, 0.3 mmol cocatalyst, 1 mL solvent, 6 h, 1 MPa CO_2.

DBN reacts with the hydroxyl hydrogen to increase the deshielding effect of the hydrogen atom, and the electron cloud density decreases and moves to the lower field.[36,37] At the same time, due to the influence of the nitrogen heteroatoms, the exchange rate of hydroxyl hydrogen slows down, and the peak is broadened.

As shown in the Fig. 8, the recyclability of Ag/ATP was evaluated. The recoverability of Ag/ATP-5 was tested with **1a** and **2a** at 50 °C (Fig. 8A). After each reaction, Ag/ATP-5 was separated from the product by a simple centrifuge and reused in subsequent reactions without any purification or cleaning. The results showed that Ag/ATP-5 could not maintain the original activity during the first cycle, and the conversion rate dropped sharply, only 7%. After the second catalytic cycle, the conversion rate was further reduced to the level in the control group (Table 3, entries 2). This indicated that the activity of Ag/ATP-5 decreased significantly in the first catalytic cycle. After the second cycle, the activity of Ag/ATP-5 almost completely disappeared.

Under specific conditions, the DBN-alcohol system absorbs CO_2 and forms ionic compounds with a carbonate structure.[36–40] We speculate that Ag/ATP-5 deactivation is due to the coating of such substances. At the same time, we also found that such compounds can decompose at higher temperatures.[36–40] So, the reaction temperature was rose to 90 °C. The purpose of this is to combine the regeneration process of the catalyst with the catalytic process and abandon the regeneration method of cleaning, which has high energy consumption and large loss of catalyst in industrial production.

The results were exactly as we expected, and Ag/ATP-5 remained active in the first catalytic cycle at 90 °C (Fig. 8B). What is more noteworthy is that in the ten consecutive catalytic reactions, the activity of Ag/ATP-5 stayed at a high level without attenuation. In addition, IR and XRD studies proved that the structure of Ag/ATP-5 was not damaged after ten consecutive catalytic reactions (Fig. S13 and S14†). This series of studies has proved that ATP, a nanometer mineral, is an excellent carrier that can stably load metal nanoparticles. This also proves the excellent reusability of Ag/ATP catalysts. By combining the regeneration process with the catalytic process, Ag/ATP-5 has great industrial potential.

According to the experimental results in this paper and related knowledge in the literature, a possible catalytic reaction mechanism (Fig. 9) is proposed.[5,6] In the previous paper, it has been proved using ^{1}H NMR that the proton hydrogen of the alcoholic hydroxyl group is taken up by DBN to form

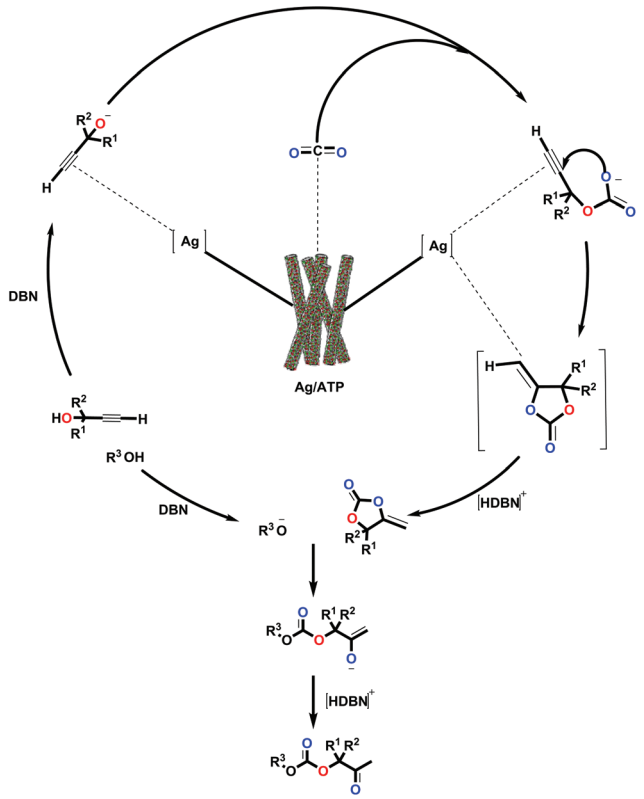

Fig. 9 The reaction mechanism.

$[DBNH]^+$. Then, the CO_2 adsorbed onto the ATP electrophilically attacks the O atom of the alkoxy group to form an ionic compound having a carbonate structure.[41] At the same time, the silver nanoparticles on the ATP activated the alkynyl group nearby, and the oxygen anion can attack the alkynyl group.[42] $[HDBN]^+$ transfers electrons to the alkynyl group, and thus the cyclic carbonate is formed. DBN continues to activate benzyl alcohol to form an oxygen anion to nucleophilically attack the carbonyl group of the intermediate, and the target product is formed by ring opening and tautomerism.

Conclusions

We take ATP as a carrier, and introduce it into the carbon dioxide fixation reaction; by taking full advantages of its size and structure, the Ag/ATP nanocomposite catalyst was designed and prepared. The catalytic activity of the catalyst in the synthesis of non-symmetric carbonate was verified by catalytic experiments, and the TOF value could reach 132 h^{-1}. The remarkable stability of the Ag/ATP nanocomposite catalyst was verified by catalytic cycle experiments that showed that it can maintain the activity for ten consecutive reactions; thus, it has a certain potential in industrial applications. Therefore, we boldly infer that, due to the excellent ability of ATP to absorb carbon dioxide gas and stabilize the surface supported substances, Ag/ATP has better stability and catalytic activity in this catalytic process compared to previous heterogeneous catalysts. In conclusion, this study not only provides an efficient and stable catalyst for CO_2 fixation but also shows that ATP is an excellent carrier and provides a new idea for the development of related heterogeneous catalysts.

Conflicts of interest

The authors declare that they have no conflict of interest.

Acknowledgements

This work was supported by the National Natural Science Foundation of China (Grant No. 21871122, 21431002) and the Fundamental Research Funds for the Central Universities (Grant No. lzujbky-2020-kb13, lzujbky-2018-kb12).

References

1 Z. H. Zhou, Q. W. Song, J. N. Xie, R. Ma and L. N. He, *Chem. – Asian J.*, 2016, **11**, 2065–2071.
2 Y. Ono, *Appl. Catal., A*, 1997, **155**, 133–166.
3 J. M. Joumier, J. Fournier, C. Bruneau and P. H. Dixneuf, *J. Chem. Soc., Perkin Trans. 1*, 1991, 3271–3274, DOI: 10.1039/P19910003271.
4 N. D. Ca, B. Gabriele, G. Ruffolo, L. Veltri, T. Zanetta and M. Costa, *Adv. Synth. Catal.*, 2011, **353**, 133–146.
5 J. Hu, J. Ma, L. Lu, Q. Qian, Z. Zhang, C. Xie and B. Han, *ChemSusChem*, 2017, **10**, 1292–1297.
6 J. Li, Q. Song, H. Zhang, P. Liu, K. Zhang, J. Wang and D. Zhang, *Tetrahedron*, 2019, **75**, 2343–2349.
7 B. W. F, *Am. Mineral.*, 1940, **25**, 405–410.
8 J. E. Post and P. J. Heaney, *Am. Mineral.*, 2008, **93**, 667–675.
9 J. Xu, W. Han, Q. Yin, J. Song and H. Zhong, *Chin. J. Chem.*, 2009, **27**, 2197–2202.
10 D. Pan, Q. Fan, F. Fan, Y. Tang, Y. Zhang and W. Wu, *Sep. Purif. Technol.*, 2017, **177**, 86–93.
11 N. Güven, J.-B. d'Espinose de la Caillerie and J. J. Fripiat, *Clays Clay Miner.*, 1992, **40**, 457–461.
12 G. Chiari, R. Giustetto and G. Ricchiardi, *Eur. J. Mineral.*, 2003, **15**, 21–33.
13 E. Galan, *Clay Miner.*, 1996, **31**, 443–453.
14 Q.-W. Song, Z.-H. Zhou, H. Yin and L.-N. He, *ChemSusChem*, 2015, **8**, 3967–3972.
15 A. Xie, X. Zhou, X. Huang, L. Ji, W. Zhou, S. Luo and C. Yao, *J. Ind. Eng. Chem.*, 2017, **49**, 230–241.
16 L. Dong, L. Lin, Q. Li, Z. Huang, X. Tang, M. Wu, C. Li, X. Cao and M. Scholz, *J. Environ. Manage.*, 2018, **213**, 151–158.
17 Z. Zhang, W. Wang, G. Tian, Q. Wang and A. Wang, *Appl. Clay Sci.*, 2018, **159**, 16–24.
18 W. Wang, Y. Kang and A. Wang, *J. Nanopart. Res.*, 2014, **16**, 2281.

19 X. Wu, W. Zhu, X. Zhang, T. Chen and R. L. Frost, *Appl. Clay Sci.*, 2011, **52**, 400–406.
20 T. Chen, H. Liu, J. Li, D. Chen, D. Chang, D. Kong and R. L. Frost, *Chem. Eng. J.*, 2011, **166**, 1017–1021.
21 X. Wang, B. Mu, A. Zhang, X. An and A. Wang, *Powder Technol.*, 2019, **343**, 68–78.
22 P. Jeevanandam, C. K. Srikanth and S. Dixit, *Mater. Chem. Phys.*, 2010, **122**, 402–407.
23 X. Li, F. Li, X. Lu, S. Zuo, Z. Li, C. Yao and C. Ni, *Powder Technol.*, 2018, **327**, 467–475.
24 X. Wang, B. Mu, X. An and A. Wang, *Appl. Surf. Sci.*, 2018, **439**, 202–212.
25 S. Ma, X. Li, X. Lu, S. Zuo, Z. Li and C. Yao, *J. Mater. Sci.: Mater. Electron.*, 2017, **29**, 2709–2715.
26 H. Zhang, X. Li, Y. Hui, L. Yu, Q. Xia, S. Luo and C. Yao, *J. Mater. Sci.: Mater. Electron.*, 2017, **28**, 9371–9377.
27 Z. Zhang, W. Wang, Y. Kang, L. Zong and A. Wang, *Appl. Clay Sci.*, 2016, **120**, 28–39.
28 R. A. Molla, K. Ghosh, B. Banerjee, M. A. Iqubal, S. K. Kundu, S. M. Islam and A. Bhaumik, *J. Colloid Interface Sci.*, 2016, **477**, 220–229.
29 Y. Wang, M. Chen, Z. Yang, T. Liang, S. Liu, Z. Zhou and X. Li, *Appl. Catal., A*, 2018, **550**, 214–227.
30 U. Shuali, S. Yariv, M. Steinberg, M. Müller-Vonmoos, G. Kahr and A. Rub, *Clay Miner.*, 1991, **26**, 497–506.
31 U. Shuali, S. Yariv, M. Steinberg, M. Müller-Vonmoos, G. Kahr and A. Rub, *Thermochim. Acta*, 1988, **135**, 291–297.
32 X. Zhou, X. Huang, A. Xie, S. Luo, C. Yao, X. Li and S. Zuo, *Chem. Eng. J.*, 2017, **326**, 1074–1085.
33 N. I. Andersen, A. Serov and P. Atanassov, *Appl. Catal., B*, 2015, **163**, 623–627.
34 E. Abdullayev, K. Sakakibara, K. Okamoto, W. Wei, K. Ariga and Y. Lvov, *ACS Appl. Mater. Interfaces*, 2011, **3**, 4040–4046.
35 P. Uznanski and E. Bryszewska, *J. Mater. Sci.*, 2009, **45**, 1547–1552.
36 M. K. Munshi, P. S. Biradar, S. M. Gade, V. H. Rane and A. A. Kelkar, *RSC Adv.*, 2014, **4**, 17124.
37 P. D. Vaidya and E. Y. Kenig, *Chem. Eng. Technol.*, 2007, **30**, 1467–1474.
38 L. Phan, D. Chiu, D. J. Heldebrant, H. Huttenhower, E. John, X. Li, P. Pollet, R. Wang, C. A. Eckert, C. L. Liotta and P. G. Jessop, *Ind. Eng. Chem. Res.*, 2008, **47**, 539–545.
39 I. Anugwom, P. Mäki-Arvela, P. Virtanen, P. Damlin, R. Sjöholm and J.-P. Mikkola, *RSC Adv.*, 2011, **1**, 452.
40 I. Anugwom, P. Mäki-Arvela, P. Virtanen, S. Willför, P. Damlin, M. Hedenström and J.-P. Mikkola, *Holzforschung*, 2012, **66**, 809–815.
41 J.-Y. Li, L.-H. Han, Q.-C. Xu, Q.-W. Song, P. Liu and K. Zhang, *ACS Sustainable Chem. Eng.*, 2019, **7**, 3378–3388.
42 Q. Wang, W. Xiong, X. Deng, X. Zhou, D. C. Qi and P. D. J. Hu, *Asian J. Org. Chem.*, 2018, **8**, 179–184.